A Numerical Investigation of Dominant Factors Affecting the Bubble Dynamics Between Air-water and CO_2-cryolite Systems

Zhibin Zhao[1,2], Kaiyu Zhang[1], Yuqing Feng[2], Peter Witt[2], Phil Schwarz[2],

Zhaowen Wang[1], Mark Cooksey[2]

[1] School of Material and Metallurgy

Northeastern University, Shenyang 110089, China

[2] Mineral Resource Flagship

CSIRO, Melbourne 3168, Australia

Abstract

Air-water models, as a substitute for CO_2-cryolite systems, have been widely applied to study the complex bubble driven liquid flow that occurs in the aluminium electrolysis process. The argument for using the air-water system is that the kinematic viscosity of water is very similar to that of cryolite (1.005×10^{-6} $m^2 \cdot s^{-1}$ for water at 20°C and 1.43×10^{-6} $m^2 \cdot s^{-1}$ for cryolite at 960°C). Thus, similar liquid flow dynamics will result as long as the same volume of gas is used. A recent study [1] showed that for a fixed bubble size, the CO_2 bubble in cryolite leads to a larger bubble sliding velocity under the anode and a smaller bubble thickness than the air bubble in water.

In this paper, the effect of property differences between the two systems was investigated in detail. The study is based on a computational fluid dynamics (CFD) model with the volume-of-fluid (VOF) method to predict the bubble shapes. It was found that the contact angle is a dominant factor affecting the bubble dynamics between the two systems. The findings will help to select substitutive systems to better understand complex flow dynamics in aluminium electrolytic cells.

Introduction

In Hall-Héroult cells, a direct current flows from carbon anodes and passes through the electrolyte-metal layers into the carbon cathode. The aluminium liquid is electrically produced from alumina on the surface of cathode, and pumped out regularly in 1-2 days. The carbon anode is consumed at a rate of about 1.5 cm per day, which produces of a gas emission about 0.002 $m^3 \cdot s^{-1} \cdot m^{-2}$ [2]. The anodic bubbles glide under the anode, and release from the anode. Obviously, the cell resistance [3,4,5,6], current distribution [2,5], alumina mixing [7], bath circulation and heat exchange [8,9,10,11] are influenced by the presence and motion of gas bubbles. A better knowledge of gas bubble dynamics is essential to increase the fundamental understandings of aluminium electrolytic process.

However, it is hard to investigate the bubble behaviour directly due to the high temperature and corrosive environment in commercial cells. As a substitute for CO_2-cryolite system, air-water models [1,3,4,6,12,13,16,17,18,19,20,21,22] have been widely applied to study the complex bubble driven liquid flow with the advantage of easier operation and measurement. In air-water models, compressed air is forced through porous material "anodes" to simulate the gas generation, while water or other aqueous solutions (adding some organic solvent to change surface tension [9,14,15]) are used as electrolyte. A detailed application of air-water models in recent decades has been reviewed in our previous works [1].

The standpoint for using the air-water system is that the kinematic viscosity of water is very similar to that of cryolite, as shown in Table 1.

Properties	CO_2 at 960°C	Cryolite at 960°C	Air at 25°C	Water at 25°C
Density (kg/m^3)	0.4	2100	1.225	998.2
Dynamic viscosity $(kg/m \cdot s)$	1.37×10^{-5}	3.0×10^{-3}	1.789×10^{-5}	1.003×10^{-3}
Kinematic viscosity (m^2/s)	3.43×10^{-5}	$\mathbf{1.43\times10^{-6}}$	1.46×10^{-5}	$\mathbf{1.005\times10^{-6}}$
Surface tension (N/m)	0.132		0.072	
Contact angle (degree)	120		60	

Table 1. Physical properties of the CO_2-cryolite and Air-water systems

With the similar kinematic viscosity, similar liquid flow dynamics will be resulted as long as the same volume of gas is used. However, the other gas and liquid properties, such as surface tension, contact angle and gas and liquid density, are quite different in the substitutive systems and the real CO_2-cryolite system. In fact, there is good evidence that the bubble shape and motion are strongly influenced by the liquid properties [24]. The question arises as to the similarity and difference between results from the two systems.

In our previous work [1], a comparison for some fixed size bubbles between the two systems was discussed based on a computational fluid dynamics (CFD) model with the volume-of-fluid (VOF) method. The results demonstrate that a larger bubble sliding velocity and a smaller bubble thickness were obtained in the CO_2-cryolite system compared to the air-water system. The bubble morphology was quite different in the two systems as well.

This paper presents additional comparison of the two systems using the CFD-VOF model to further investigate relationship between properties and bubble dynamics. The CFD-VOF model is based on similar simulation conditions to those of the previous studies [1]. The mesh adaption technology is optimized from

level 4 to level 3 for saving computing time and resource in this work.

Dimensionless Analysis and Model Description

Dimensionless Analysis

For a bubble moving in surrounding liquid, it is possible to identify three important dimensionless numbers to describe its behaviour. These numbers are listed as following:

Reynolds number: $\mathrm{Re} = \dfrac{\rho \upsilon d}{\mu}$

Eötvös number: $Eo = \dfrac{\Delta \rho g d^2}{\sigma}$

Morton number: $Mo = \dfrac{\Delta \rho g \mu^4}{\rho^2 \sigma^3}$

where, ρ, μ and σ are the liquid density, viscosity and surface tension respectively; v and d are the bubble velocity and equivalent diameter; the term $\Delta \rho$ is the density difference between the liquid and gas bubbles; g is the gravitational acceleration.

In such a case, the function of bubble morphology and motion can be expressed as an equation:

$$F_{bubble} = f(Mo, Eo, \mathrm{Re}, \theta, \mathrm{X}) \qquad (1)$$

where, θ is the gas-liquid contact angle on the anode surface, X stands for all other factors, such as surface heterogeneity, surface roughness and anode inclination.

Introducing another two dimensionless numbers ($We = \dfrac{\rho \upsilon^2 d}{\sigma}$

and $Fr = \dfrac{\rho \upsilon^2}{\Delta \rho g d}$) into equation (1) based on the forms of

$Eo = \dfrac{We}{Fr}$ and $Mo = \dfrac{We^3}{Fr \times \mathrm{Re}^4}$, the above equation (1) could be described as:

$$F_{bubble} = F(\mathrm{Re}, We, Fr, \theta, \mathrm{X}) \quad (2)$$

In equation (2), the three dimensionless numbers also could be identified by the ratio of bubble controlled forces. The following equations give the details of each number here.

Reynolds number: $\mathrm{Re} = 12 \times \dfrac{\text{Inertial Force}}{\text{Viscosity Force}}$

Weber Number: $We = \dfrac{2}{3} \times \dfrac{\text{Inertial Force}}{\text{Surface Tension Force}}$

Froude Number: $Fr = 4 \times \dfrac{\text{Inertial Force}}{\text{Buoyancy Force}}$

where the inertial force is expressed as $\dfrac{\pi}{4} \times \rho \upsilon^2 d^2$; the viscosity force is defined as $3 \times \pi \times \mu \upsilon d$; the surface tension force is presented by $\pi \times \sigma d$; the buoyancy force is described as $\dfrac{\pi}{6} \times \Delta \rho g d^3$.

For the fixed bubble, Re number describes the viscosity effect in two systems; the We number expresses the surface tension effect; the Fr number refers the density difference of liquid and gas in two systems.

$$\mathrm{Re} = \frac{\rho \upsilon d}{\mu} = \frac{\upsilon d}{\mu / \rho}$$

$$We = \frac{\rho \upsilon^2 d}{\sigma} = \frac{\upsilon^2 d}{\sigma / \rho}$$

It is surprising to notice that the controlling item (μ/ρ and σ/ρ) of the two dimensionless numbers are very close in values (μ/ρ is 1.43×10^{-6} for cryolite at 960 ℃ and 1.005×10^{-6} for water at 25 ℃; σ/ρ is 6.29×10^{-5} for cryolite at 960 ℃ and 7.21×10^{-5} for water at 25 ℃). This indicates the effect of the viscosity and surface tension difference play little role on bubble dynamics difference.

In order to investigate the effect of density difference and contact angle difference, a case table was made for modelling, as shown in Table 2.

System \ Contact angle	60°	120°
Air-water	Case 1	Case 2
CO$_2$-cryolite	Case 3	——

Table 2. Simulation cases with different setting

The effect of surface heterogeneity, surface roughness and anode inclination (item X in equation 2) was not discussed here, as all these parameters were set the same in all cases.

The contact angle of CO_2 bubble on carbon anode in electrolyte is about 60°, and that is 120° for air bubble on plexiglass in water. In addition to the real air-water system (case 2) and CO_2-cryolite system (case 3), an assumptive air-water case with contact angle 60 setting (case 1) was established.

The resultant comparison of case 1 and case 2 (same system, different contact angle) is to investigate the effect of contact angle, while the comparison of case 1 and case 3 (different system, same contact angle) is to focus on the effect of density difference.

Model Description

The CFD-VOF model was well described in previous work [1]. Here, only a brief description is provided. The inlet boundary is 5 mm length with an inlet velocity of 0.25 m/s for a fixed injection time of 0.32 s. The equivalent diameter of the bubble is 22.6 mm after gas injection in three cases. The only difference with the previous model is the mesh adaption scheme, decreased from level 4 to level 3 to save computing resources and time. Figure 1 shows the sliding velocity and morphologies in different mesh-adaption cases. Little difference is found between the two cases.
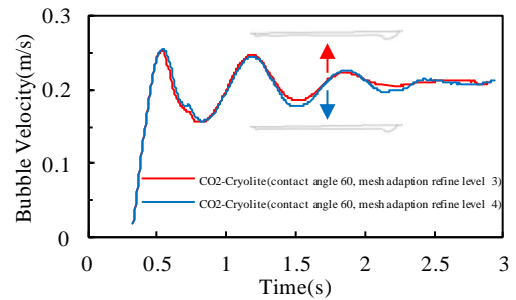
Figure 1. The sliding velocity and morphology of gas bubble for different mesh-adaption cases

Results and Discussion

The bubble behaviour can be divided into three stages: bubble growth at the nucleation site, bubble sliding alone the anode bottom and bubble rising in the side channel. The effect of properties on bubble dynamics is analysed for each of the three stages here.

Bubble Growth

The three cases with different settings were simulated by the commercial software ANSYS-Fluent with the VOF model. In this study, gas is injected into the liquid to simulate gas generation. The growth morphologies of bubbles at different times (0.005s, 0.01s, 0.02s, 0.03s, 0.04s, 0.06s, 0.1s) are plotted in Figure 2.

(a)

(b)

(c)
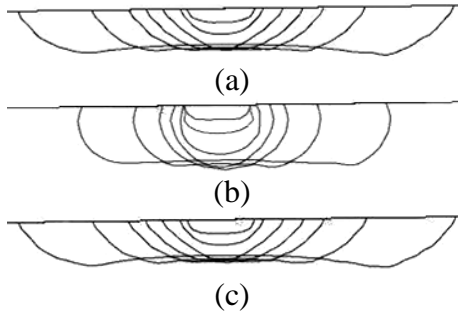
Figure 2. Bubble growth morphologies for different cases   (a), case 1 Air-water (contact angle 60°)   (b), case 2 Air-water (contact angle 120°) (c), case 3 CO_2-cryolite (contact angle 60°)

Initially, a single bubble grows at the nucleation point due to the gas injection. A change of half-ellipsoidal to half-spherical shape on bubbles occurs following continued gas injection. When the bubble diameter grows to a certain value (the maximum thickness), the bubble is squeezed to a flat shape by buoyancy, forming a 'pancake' shape. Then, the bubble expands along the surface rapidly. In such a process, the bubble maintains symmetry about the inlet axis, which means the small inclination angle of anode (1.5°) has little influence on bubble formation in this stage.

It also can be seen that the bubble shape in case 1 and case 3 is surprisingly similar, both of them quite different with that in case 2.   The bubbles attach more closely to the anode bottom in case 1 and 3 due to the lack of wettability of liquid on the anode surface. Comparison of case 1 and case 3 implies the effect of density difference of gas and liquid on bubble dynamics is very small.

Since the bubbles are irregular and complex in shape, the mean bubble thickness would provide more information of the bubble growth characteristic.
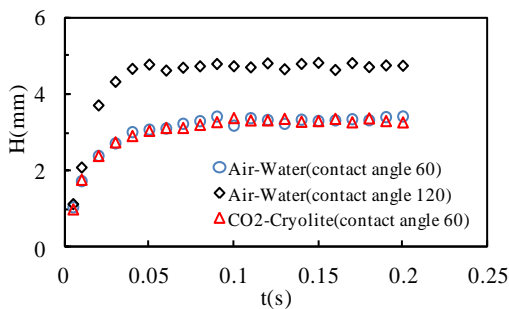
Figure 3. Bubble layer thickness growth curve

Figure 3 shows the functions of bubble thickness with time for all simulation cases in air-water system and CO_2-cryolite system. For all cases, the bubble thickness grows rapidly at first,

increases slowly after a period of time and finally reaches a maximum value (h_{max}). Then, a slight decrease of bubble depth occurs in three cases (h_{lim}), the bubble layer maintaining a stable level after that.

According to Hartland [22], the formulas for the maximum and limiting thickness of a stationary bubble under a downward surface were given:

$$h_{max} = (-0.19 \times (\pi - \theta)^2 + 1.293 \times (\pi - \theta) - 0.053) \times \sqrt{\frac{\sigma}{(\rho_l - \rho_g)g}} \qquad (3)$$

$$h_{lim} = \sqrt{2 \times (1 - \cos(\pi - \theta))} \times \sqrt{\frac{\sigma}{(\rho_l - \rho_g)g}} \qquad (4)$$

where θ is the contact angle.

Zhang [1] calculated the maximum and limiting heights of CO_2 bubbles in molten cryolite to be 2.8 mm and 2.5 mm, and that of air bubbles in water to be 4.9 mm and 4.7 mm. These results are agreed with our simulation. With the same equations, Vekony [20] calculated the maximum and limiting heights of 4.19 mm and 3.95 mm in molten cryolite and 4.44 mm and 4.18mm in water. As the term $\sqrt{\frac{\sigma}{(\rho_l - \rho_g)g}}$ on the right hand side of equation (3) and (4) gives a similar value for the two systems, the difference of CO_2 bubble thickness (about 1.4 mm) in their studies resulted from the only difference - the contact angle.

Figure 2 and Figure 3 show the difference in bubble growth is dominated by the contact angle obviously.

Bubble sliding

The large bubbles travel along the inclined anode surface, coalescing with any small bubbles they encounter [13,19]. The motion of bubbles plays an important role in driving electrolyte flow. In this section, the bubbles are qualified by their morphology and velocity to investigate the dominant factor in bubble difference.

In Figure 4, bubble morphologies for the same case at different times show a high degree of similarity. The bubbles present a bigger thickness and a smaller length in cases 2 than that in case 1 and case 3 for the same size bubbles. The contact angle dominates the bubble difference just as it does in bubble growth stage.

(a)

(b)

(c)
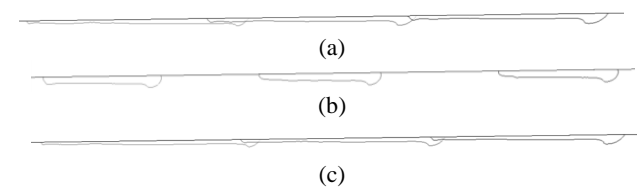
Figure 4. Bubbles sliding underneath the anode in different times   (a), case 1 Air-water (contact angle 60°)   (b), case 2 Air-water (contact angle 120°)   (c), case 3 CO_2-cryolite (contact angle 60°)
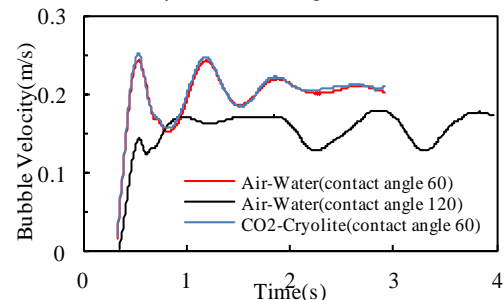
Figure 5. Bubble sliding velocity as function of time   (a), case 1 Air-water (contact angle 60°)   (b), case 2 Air-water (contact angle 120°) (c), case 3 CO_2-cryolite (contact angle 60°)

Figure 5 shows the bubble sliding velocity along the anode bottom in three cases. As gas injection stops, the bubble starts to slide along the inclination anode under the combined effects of skin friction and buoyancy. After reaching to the peak velocity, the velocity drops to the smaller value, and then increases for next fluctuation. The velocity curve in case 1 is very consistent with that in case 3. But there is a significant decrease in the velocity in case 2.

The mean velocity and terminal velocity of bubbles is shown in Table 3. The similar velocities in case 1 and 3 indicates the effect of density difference plays little role in bubble motion difference. While the velocity in case 2 is slightly lower than that in the case 2 that implies that the dominate factor in bubble sliding process is the contact angle.

System \ Contact angle	60°		120°	
	Mean Velocity	Terminal Velocity	Mean Velocity	Terminal Velocity
Air-water	0.199m/s	0.203m/s	0.155m/s	0.173m/s
CO_2-cryolite	0.202m/s	0.210m/s	——	——

Table 3. Bubble mean and terminal velocity in different cases

The velocity difference is due to the bubble shape difference: with a smaller thickness and a sharper head, the sliding bubble receives a smaller friction on the gas-liquid interface. Consequently, the resistance around the bubble is smaller in case 1 than that in case 2.

Figure 4 and Figure 5 illustrate the contact angle plays a more important role than density difference in bubble sliding stage.

Bubble rising

As bubbles release from anode edge, the bubbles rise in the side channel until escaping from the liquid. The release of bubbles is not only a main driver for the circulation of electrolyte, it can also introduces some fluctuations at the metal-bath interface.

Figure 6 shows the bubble morphologies in the side channel at three different times for each case. It can be seen the bubbles break into smaller ones while rising. The small bubbles closely follow their parental bubbles for some time. Similar bubble morphology is shown in case 1 and case 3, in which the bubbles climb along the side wall all the way. Conversely, the bubble in case 2 climbs along the side wall at the beginning, and detaches away from the side wall later. Some gas is trapped at the edge. The trapped gas in case 1 and case 3 is obviously more than that in case 2. On the other hand, the rising bubble in case 2 is bigger.

The mean velocities of bubbles in three different cases also are shown in Figure 6. The velocity in case 1 is close to that in case 3. Both of them are larger than the velocity in case 2. From the comparison of case 1 and case 2, the effect of contact angle can be seen: the bubble morphologies are quite different between two cases, and the bubble velocity is smaller in case 2 as well. The morphology difference is responsible for the velocity difference.

With the same contact angle, the bubble velocity in the CO_2-cryolite system is a slightly larger than that in air-water system (comparison of case 1 and case 3). This may due to subtle difference in bubble shape resulting from different kinematic viscosity or relative density.

The comparison shows the contact angle plays a dominant role in determining the difference in bubble rising stage.

3.00s   3.25s   3.45s
Rising Velocity: 0.261m/s

(a)

4.10s   4.35s   4.60s
Rising Velocity: 0.205m/s

(b)

3.00s   3.25s   3.45s
Rising Velocity: 0.263m/s

(c)
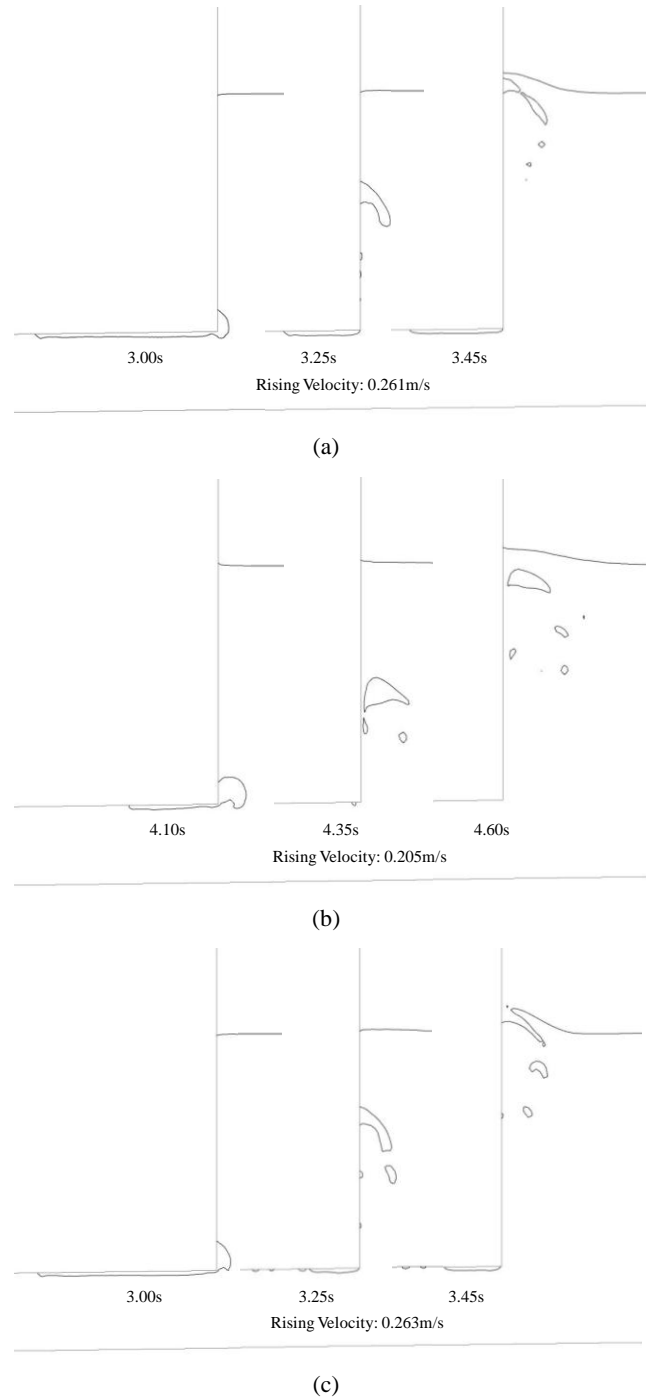
Figure 6. Bubbles rising in the side channel   (a), case 1 Air-water (contact angle 60°)   (b), case 2 Air-water (contact angle 120°)   (c), case 3 CO_2-cryolite (contact angle 60°)

Conclusions

This work investigates the effect of the property difference on the bubble dynamics differences between the CO_2-cryolite and Air-water systems.

From the dimensionless analysis, the Re number and *We* number are quite similar in two systems that indicates the effect of viscosity and surface tension would be very small. The other properties (density difference and contact angle) were studied using an advanced VOF-CFD model with mesh adaption technology.

This work solved the problems presented in previous paper [1]. The larger sliding velocity and smaller thickness of CO_2 bubbles in cryolite compared with air bubbles in water is due to the difference in the contact angle. With lower contact angle, the bubble has a smaller thickness and a sharper head. In such a case, a higher sliding velocity is resulted due to the smaller resistance in the surrounding liquid.

The contact angle also plays a dominant role in bubble rising. In the same air-water system, the bubble climbs along the anode side wall in case 1, while the bubbles detach from the side wall after a period of time and rise freely in liquid in case 2. The rising velocity is smaller in case 2 as well, which is due to the morphology difference.

This work has identified the dominant factors affecting the difference in bubble dynamics between the two systems. The findings will be helpful in selecting the substitutive systems (for example, changing the contact angle of the air-water system), which would provide a better understanding of the complex flow dynamics in aluminium electrolytic cells.

References

[1] Zhang, K.Y., Feng Y.Q & Schwarz, M.P., Computational Fluid Dynamics (CFD) Modelling of Bubble Dynamics in the Aluminum Smelting Process, *Industrial &Engineering Chemistry Research*, **52**, 2013, 11378-11390.

[2] Zoric, J. & Solheim, A., On Gas Bubbles in Industrial Aluminium Cells with Prebaked Anodes and Their Influence on the Current Distribution, *Journal of Applied Electrochemistry*, **30**, 2000, 787-794.

[3] Qian, K. & Chen, J.J.J., Visual Observation of Bubbles at Horizontal Electrodes and Resistance Measurement on Vertical Electrodes, *Journal of Applied Electrochemistry*, 27, 1997, 434-440.

[4] Qian, K., Chen Z.D. & Chen, J.J.J., Bubble Coverage and Bubble Resistance Using Cells with Horizontal Electrode, *Journal of Applied Electrochemistry*, **28**, 1998, 1141-1145.

[5] Zhang K.Y., Feng Y.Q. & Peter J.W., A Numerical Assessment of Bubble Induced Voltage Drop and Current Flow in Aluminum Electrolytic Cells, accepted by *Journal of Applied Electrochemistry*, 2014.

[6] Perron, A.L., Kiss, L.I. & Poncsak, S., Mathematical Model to Evaluate the Ohmic Resistance Caused by the Presence of a Large Number of Bubbles in Hall-Héroult Cells, *Journal of Applied Electrochemistry*, **37**, 2007, 303-310.

[7] Feng, Y.Q., Cooksey, M.A. & Schwarz, M.P., CFD Modelling of Alumina Mixing in Aluminium Reduction Cells, *Light Metals*, 2011, 543-548.

[8] Feng, Y.Q., Cooksey, M.A. & Schwarz, M.P., CFD Modelling of Electrolyte Flow in Aluminium Reduction Cells, *Light Metals*, 2007, 339-344.

[9] Solheim, A., Jonansen, S.T. & Rolseth, S., Gas Induced Bath Circulation in Aluminium Reduction Cells, *Journal of Applied Electrochemistry*, **19**, 1989, 703-712.

[10] Solheim, A., Jonansen, S.T. & Rolseth, S., Gas Driven Flow in Hall-Heroult Cells, *Light Metals*, 1989, 245-252.

[11] Zhou, N.J., Xia, X.X. & Bao, S.Z., Effect of Electromagnetic Force and Anode Gas on Electrolyte Flow in Aluminium Electrolysis Cell, *Journal of Central South University of Technology*, **13**, 2006, 496-500.

[12] Dernedde, E. & Canbridge, E.L., Gas Induced Circulation in an Aluminium Reduction Cell, *Light Metals*, 111-119

[13] Fortin, S., Gerhardt, M. & Gesing, A.J., Physical Modelling of Bubble Behaviour and Gas-release From Aluminium Reduction Cell Anodes. *Light Metals*. 1984, 721-741.

[14] Shekhar, R. & Evans, J.W., Physical Modelling Studies of Electrolyte Flow Due to Gas Evolution and Some Aspects of Bubble Behaviour in Advanced Hall Cells Part I: Flow in Cells with a Flat Anode, *Metallurgical and Materials Transactions B*, **25**, 1994, 333-340.

[15] Perron, A., Kiss, L.I. & Poncsak, S., Motion of Singles Bubbles Moving under a Slightly Inclined Surface Through Stationary Liquids, *International Journal of Multiphase Flow*, **32**, 2006, 1311-1325.

[16] Che, D.F., Chen, J.J.J. & Taylor, M.P., Gas Bubble Formation and Rise Velocity Beneath a Downward Facing Inclined Surface Submerged in a Liquid, *Chemical engineering research & design*, **69**, 1991, 25-29.

[17] Chen, J.J.J., Shen, X.C. & M.P. Taylor, A Study of Bath Velocity Distribution in a 3-D Water Model, *Light Metals*, 1996, 343-350.

[18] Chen, J.J.J., Qian, K.X. & Zhao, J.C., Resistance Due to the Presence of Bubbles in an Electrolytic Cell with a Grooved Anode, *Chemical Engineering Research and Design*, **79**, 2001, 383-388.

[19] Poncsak, S., Kiss, L.I. & Toulouse, D., Size Distribution of the Bubbles in the Hall-Heroult cells, *Light Metals*, 2006, 457-462.

[20] Vekony, K. & Kiss, L.I., Morphology of Two-phase Layers with Large Bubbles, *Metallurgical and materials transaction B*, **41**, 2010, 1006-1017.

[21] Vekony, K. & Kiss, L.I., Experimental Study of the Morphology and Dynamics of Gas-laden Layers under the Anodes in an Air-water Model of Aluminium Reduction Cells, *Metallurgical and materials transaction B*, **43**, 2012, 1086-1097.

[22] Kiss, L.I. & Poncsak, S., Effect of the Bubble Growth Mechanism on the Spectrum of Voltage Fluctuations in the Reduction Cell, *Light Metals*, 2002, 402-408.

[23] Hartland, S. & Hartley, R.W. (editor) *Axisymmetric fluid-liquid interfaces: tables giving the shape of sessile and pendant drops and external menisci, with examples of their use* New York, Elsevier Scientific Publishing Co., 1976.

[24] Das, S., Morsi, Y.S. & Brooks, G., Principal Characteristics of a Bubble Formation on a Horizontal Downward Facing Surface, *Colloids and surface A: Physicochem. Eng. Aspects*, **411**, 2012, 94-104.